Harnessing Random Peptide Mixtures to Overcome Multidrug-Resistant Fungal Infections

Authors list: John Adeoye*[1], Yael Bello*[2], Marina Campos Rocha[1], Hilla Hayby[1], Aygun Israyilova[3], Zvi Hayouka[2], Neta Shlezinger[1]

Affiliations: [1] Koret School of Veterinary Medicine, Faculty of Agriculture, The Hebrew University, Rehovot, Israel

[2] Institute of Biochemistry, Food Science and Nutrition, The Robert H. Smith Faculty of Agricultural, Food & Environment, The Hebrew University of Jerusalem, Rehovot, Israel

[3] Laboratory of Microbiology, Center for Excellence in Research, Development & Innovation, Baku State University, Baku, Azerbaijan

Corresponding author: neta.shlezinger1@mail.huji.ac.il, zvi.hayouka@mail.huji.ac.il

Keywords: Antifungals, *Candida auris*, AMPs, candidiasis, AMR

*Co-first authors

Abstract

Invasive fungal infections, characterized by high mortality rates, present a growing health concern due to the limited spectrum of effective drugs, escalating numbers of immunocompromised patients, and the rapid emergence of drug resistance. Addressing this challenge requires alternative therapeutic strategies. Candidate drugs should fulfill key requirements to qualify for clinical use, including negligible host toxicity, high *in vitro* and *in vivo* antifungal activity, *in vivo* stability, and modes of action that reduce the potential for the emergence of resistant strains. Antimicrobial peptides (AMPs) stand out as a promising class of compounds to combat antimicrobial resistance. Leveraging the unique properties of AMPs, we previously developed a novel approach to synthesize random peptide mixtures (RPMs) with robust bactericidal activity against drug-resistant bacteria. Here, we evaluate the antifungal potential of RPMs. Our findings demonstrate high potency of FK20 (L-Phenylalanine−L-Lysine, 20-mer) RPM against *Candida auris*, a newly emerged multidrug-resistant human pathogen. *In vitro* studies demonstrated effective eradication of *C. auris*, with scanning electron microscopy revealing outer membrane damage and confocal microscopy confirming cellular penetration. FK20 also demonstrates activity against *C. albicans*, *C. glabrata*, and *C. parapsilosis*, broadening therapeutic scope. Importantly, experimental evolution assays confirm FK20 RPM hinders resistance development in *C. auris*. A synergistic activity was observed when FK20 treatment

was combined with caspofungin to inhibit *C. auris* biofilm formation. Lastly, we demonstrate the significant therapeutic potential of FK20 RPM in a murine model of systemic candidiasis. Our findings underscore the promise of RPMs as novel, efficacious, and safe treatment for drug-resistant fungal infections.

Importance

The rising prevalence of invasive fungal infections, particularly among immunocompromised individuals, has become a critical public health concern. However, antifungal drug development has not kept pace with this growing need, and treatment options remain limited to a small number of drug classes. The emergence of multidrug-resistant fungal pathogens, such as *Candida auris*, further exacerbates this crisis by reducing the efficacy of existing therapeutics and increasing the risk of treatment failure. In this study, we evaluate the antifungal potential of FK20, a random peptide mixture (RPM) composed of L-phenylalanine and L-lysine. FK20 displays potent activity against *C. auris* and other clinically relevant *Candida* species, impairs biofilm formation, and exhibits synergy with caspofungin. Importantly, FK20 limits the emergence of resistance and demonstrates therapeutic efficacy in a murine model of systemic candidiasis. These findings establish RPMs as a promising new class of antifungals with broad-spectrum activity and clinical potential against drug-resistant fungal infections.

Introduction

The surge in antimicrobial resistance poses a significant threat to public health (1–4). While attention has predominantly centered on pan-resistant bacteria, mounting apprehension surrounds multidrug-resistant fungal pathogens, notably *Candida auris*. This emerging pathogen poses a significant global health threat due to its rapid worldwide spread and intrinsic multidrug resistance (5, 6).The U.S. Centers for Disease Control and Prevention classified *C. auris* as one of only five pathogens posing the most urgent threat to public health in their 2019 Antibiotic Resistance Threats Report (7), underscoring the necessity for additional therapeutic options to address drug-resistant fungal infections.

C. auris was initially identified in 2009 in a Japanese hospital, where it was isolated from the external ear canal of a patient (8). Since then, genomic analysis has shed light on the concurrent emergence of distinct lineages, categorizing them into six major geographical clades across six continents over the past ~400 years (9–12). Its rapid transmission within clinical settings is attributed to its remarkable long-term persistence on surfaces, including human skin, as well as the widespread prevalence of drug-resistant isolates(13). Hospital-acquired *C. auris* infections, represented primarily by candidemia, typically ensue after skin colonization in patients, with mortality rates ranging from 30% to 60% (14, 15). Risk factors that increase susceptibility to *C. auris* infections are shared with other fungal infections and include iatrogenic, primary, or acquired immunodeficiency, prolonged antibiotic regimens, prolonged hospitalization, and invasive medical procedures (16).

C. auris is classified as a 'superbug fungus', posing an increasingly concerning threat to human health due to varying levels of intrinsic resistance. Approximately 5-10% of isolates exhibit resistance to all three major antifungal drug classes commonly used in clinical settings (17, 18). It is evident that over 80% of *C. auris* isolates are resistant to azole antifungals (14), and many strains exhibit notably elevated Minimum Inhibitory Concentrations (MIC) for polyenes such as Amphotericin B (19–21). For these reasons, echinocandins such as caspofungin, are used as front-line therapeutics against systemic candidemia caused by *C. auris* (22–24). However, *C. auris* isolates with a reduced susceptibility to one or more drugs in the echinocandin class have also been detected (14, 25, 26). Similar to the other *candida* species, *C. auris* employs diverse drug resistance mechanisms, including genomic point mutations or large-scale chromosomal changes that alter drug targets, and duplications of efflux pumps or their regulators. Comprehensively, the coexisting features of multidrug resistance, rapid global emergence, and heightened mortality rates collectively designate *C. auris* as a pathogen of significant concern and complexity. Thus, there is an urgent need to develop new and sophisticated antifungals to fight against *C. auris*.

Antimicrobial peptides (AMPs) stand as integral components within the immune systems of diverse organisms (27). They are characterized by short sequences composed of cationic and hydrophobic

residues, which grant them a multifaceted spectrum of activity (28, 29). AMPs play a pivotal role in immune defense by disrupting membrane integrity through the disruption of membrane of the invading pathogens (30). Building on the principles of AMPs, we have innovated the development of a novel class of antimicrobial peptides known as Random Peptide Mixtures (RPMs). Our approach involves the solid-phase synthesis of these peptides, where in each coupling step we introduce a mixture of two amino acids, one cationic and one hydrophobic (31). This method imparts increased variability, while preserving peptides' defined chain length, stereochemistry and overall composition. RPMs have exhibited remarkable antimicrobial efficacy against both Gram-positive and Gram-negative bacteria in vitro and in mice model (32–36). Here, we present for the first time, the potential of RPMs as antifungal drugs against the challenging fungal pathogen *C. auris*.

Results

Random Peptide Mixtures Demonstrate Strong Antifungal Activity against *C. auris In Vitro*

To elucidate the antifungal efficacy of random peptide mixtures (RPMs) against *C. auris*, killing assays were conducted to compare RPMs based on their amino acid composition, chain length and stereochromy. Among the tested RPMs of cationic and hydrophobic amino acids, FK20 (L-Phenylalanine−L-Lysine, 20-mer) exhibited superior antifungal activity when compared to LK20 (L-Leucine−L-Lysine, 20-mer) or IK20 (L-Isoleucine-L-Lysine, 20-mer) (Figure 1A). Given its minimal antifungal activity against *C. auris*, IK20 was selected as the negative control RPM. To further explore RPM optimization, the antifungal efficacy of FK RPMs with varying chain lengths was assessed (Figure 1B). The 5 and 10-mer FK RPMs did not exhibit any discernible antifungal properties, whereas the 30-mer FK RPM showed marginal activity. In contrast, the FK20 RPM demonstrated the highest antifungal activity, consistent with its previously reported antibacterial activity (37). Next, the impact of FK RPM stereochemistry was assessed (Figure 1C). Three stereoisomers were compared: FK20 (L-Phenylalanine−L-Lysine, 20-mer), FdK20 (L-Phenylalanine−D-Lysine, 20-mer), and dFdK20 (D-Phenylalanine−D-Lysine, 20-mer). The homochiral RPMs, FK20 and dFdK20, exhibited robust antifungal activity against *C. auris*, whereas the heterochiral RPM FdK20 displayed comparatively lower activity levels. To explore additional modifications, the antifungal activity of 5-mer FK RPMs conjugated to palmitic acid, a posttranslational lipophilic modification known to enhance the antibacterial activity of RPMs (38), was assessed (Figure 1D). These 5-mer FK lipophilic RPMs demonstrated limited antifungal activity. Based on these findings, homochiral FK20 RPM was identified as the most effective candidate for combating *C. auris* and was selected for all subsequent experiments.

FK20 RPM shows conserved efficacy across diverse *Candida* species

To assess the therapeutic versatility of FK20 RPM, its antifungal efficacy of FK20 RPM was evaluated against clinical isolates of *C. auris* and other clinically relevant *Candida* species, including *C. albicans*, *C. parapsilosis*, and *C. glabrata*. Cells were treated with either 200µg/ml FK20, IK20 RPM (negative control), or PBS control. Treatment with FK20 RPM demonstrated robust antifungal activity, effectively eliminating clinical isolates of *C. auris* (Figure 2A), *C. albicans* (Figure 2B), *C. parapsilosis* (Figure 2C), and *C. glabrata* (Figure 2D). These findings indicate that FK20 RPM maintains potent antifungal activity across diverse *Candida* species of clinical significance.

FK20 RPM Disrupts *Candida auris via* Cell Wall Penetration, Membrane Damage, ROS Induction, and Depolarization

To elucidate the mechanisms underlying FK20 RPM's antifungal activity, its ability to penetrate *C. auris* cells was assessed using N-terminally 5(6)-Carboxyfluorescein-labeled FK20 RPM. *C. auris* cells incubated with fluorescently labeled FK20 for 45 min and stained with Calcofluor White, were

visualized by confocal microscopy. Fluorescein labeled FK20 RPM (green) was observed within *C. auris* cells, surrounded by the Calcofluor White-stained cell wall (blue) (Figure 3; Supplementary Movie 1), suggesting that FK20 compromises the cell wall to facilitate entry. To investigate cell surface interactions, Scanning Electron Microscopy (SEM) was performed on *C. auris* cells incubated with 200 µg/ml of FK20 RPM stereoisomers (Figure 4). Homochiral RPMs (FK20 and dFdK20) induced significant cell surface damage and massive aggregation compared to the heterochiral FdK20 RPM and control, indicating that homochiral configurations enhance surface disruption. The impact of FK20 RPM on *C. auris* cell membrane integrity was further characterized using Propidium Iodide (PI), a fluorescent dye that penetrated compromised or damaged membranes and stain nucleic acid (39, 40). In a killing assay with increasing FK20 concentrations, followed by PI staining and flow cytometry analysis, a concentration-dependent increase PI uptake was observed, confirming escalating membrane damage (Figure 5A). Similar results were obtained with Ghost Dye, an amine-reactive viability dye (Figure S1), reinforcing these findings. Given that antimicrobial peptides as well as many membrane-targeting antibiotics often induce generation of reactive oxygen species (ROS) and membrane depolarization (41, 42), ROS generation was assessed using dihydrorhodamine 123 (DHR123) staining (Figure 5B). FK20-treated *C. auris* exhibited increased DHR123 fluorescence, confirming ROS induction. Additionally, cell membrane depolarization was evaluated using bis-(1,3-dibutylbarbituric Acid) pentamethine oxonol ($DIBAC_4(5)$), an anionic potential-sensitive dye that accumulates in depolarized cells . Increased $DiBAC_4(5)$ fluorescence in FK20-treated cells indicated significant FK20-mediated membrane depolarization (Figure 5C). Collectively, these results demonstrate that FK20 RPM exerts antifungal activity against *C. auris* by compromising and penetrating fungal cell wall, inducing ROS generation, and causing membrane depolarization.

FK20 RPM Evades *C. auris* Resistance and Benefits from Collateral Sensitivity in Caspofungin-Resistant Strains

The rapid evolution of drug resistance in pathogens is a primary cause of treatment failure, often diminishing the efficacy of new antifungals shortly after market entry. Evaluating a drug candidate's resistance potential is therefore critical. Our previous studies on the antibacterial activity of RPMs demonstrated that bacteria were unable to develop resistance, suggesting a promising low-resistance potential for this class of compounds (43, 44). To investigate the potential of *C. auris* to acquire resistance against FK20 RPM, *in vitro* experimental evolution was conducted following established protocols with minor modifications (45) (Figure 6 A). The FK20 RPM MIC_{50}, defined as the drug concentration inhibiting growth by at least 50% relative to drug-free control, was first determined (Figure S2 A). Three parallel *C. auris* lineages were evolved in RPMI-1640 media containing FK20 RPM (100 µg/ml, MIC_{50}), caspofungin (2.0 µg/ml, MIC_{50}), or no drug (ND-Evol) through ten serial passages, diluted 1:1,000 every 72 hours, resulting in the emergence of three independently evolved strains for each condition. Evolved strains were then challenged with their respective antifungal

agents, and growth kinetics were measured as optical density (OD) after 72 hours to determine new MIC_{50} values, compared to parental and ND-Evol strains. FK20-evolved strains showed no significant change in the FK20 MIC_{50} relative to parental or ND-Evol strains (Figure 6B, Figure S2 B-C). In contrast, caspofungin-evolved strains exhibited a marked increase in caspofungin MIC_{50} to >10 µg/ml (Figure 6C, Figure S2D–E). These findings demonstrate that while *C. aur*is rapidly develops resistance to caspofungin within ten passages, it fails to evolve resistance to FK20 RPM over the same timeframe, highlighting FK20's potential to limit resistance development.

Collateral sensitivity, an evolutionary trade-off where resistance to one antifungal agent increases susceptibility to another (46), was by assessing the resistance profiles of FK20-evolved and caspofungin-evolved *C. auris* strains when challenged with the reciprocal antifungal (caspofungin or FK20 RPM, respectively). FK20-evolved strains show no significant change in caspofungin MIC_{50} compared to parental or ND-Evol strains (Figure 6E, Figure S2 H-I). In contrast, caspofungin-evolved strains exhibited a marked reduction in FK20 RPM MIC-50 (Figure 6D, Figure S2 F-G), indicating collateral sensitivity to FK20 RPM. These findings suggest that while FK20 exposure does not alter caspofungin susceptibility, caspofungin resistance enhances susceptibility to FK20 RPM, a property with potential therapeutic applications.

FK20 RPM and Caspofungin are Synergistic and Inhibit *C. auris* Biofilm Formation

Combination therapies leveraging collateral sensitivity can reduce resistance evolution, as mutations conferring resistance to one antifungal may increase susceptibility to another (47). Given the observed collateral sensitivity to FK20 RPM in caspofungin-resistant *Candida auris* strains, the potential synergistic interaction between FK20 RPM and caspofungin was investigated. FK20 disrupts *C. auris* cell walls and membranes, while caspofungin inhibits the enzyme (1→3)-β-D-glucan synthase, compromising cell wall integrity (48). It was hypothesized that their combined treatment would induce synergistic cell wall damage and osmotic stress. A checkerboard assay was conducted, challenging *C. auris* cells with FK20 RPM (0–200 µg/ml) and caspofungin (0–3.2 µg/ml). The MIC_{50} values for FK20 RPM and caspofungin in combination were 3.125 µg/ml and 1.05 µg/ml, respectively (Figure 7A). The fractional inhibitory concentration index (FICI), calculated using established methods (49), yielded a value of 0.378, confirming a synergistic interaction between FK20 RPM and caspofungin.

Biofilm formation is a critical virulence factor in *Candida* species, contributing to *C. auris* pathogenicity and patient mortality (50). However, caspofungin exhibits limited efficacy against *C. auris* biofilms, requiring concentrations (>32 µg/mL for 90% inhibition) that exceeds safe clinical doses (50, 51). Given the synergistic interaction between FK20 RPM and caspofungin, their combined potential to inhibit biofilm formation was evaluated. A biofilm inhibition assay was conducted by culturing *C. auris* cells in a polystyrene 96-well plate with varying concentrations of FK20 RPM, caspofungin, or their combinations. After 24 hours, biofilms were quantified using MTT and crystal

violet assays (Figure 7B-C). Individually caspofungin and FK20 reduced biofilm formation with increasing concentrations, achieving complete inhibition at 200 µg/ml (FK20, crystal violet) and 12.8 µg/ml (caspofungin, MTT), respectively. Neither agent inhibited biofilm formation at low concentrations. In contrast, four combinations of FK20 RPM and caspofungin, at concentrations 32-fold and 15-fold lower than their respective MICs, completely inhibited biofilm formation. These findings highlight the potent synergistic efficacy of FK20 and caspofungin in preventing *C. auris* biofilm formation at clinically relevant concentrations.

FK20 RPM demonstrates therapeutic promise in a murine candidiasis model

To evaluate the therapeutic potential of FK20 RPM, its cytotoxicity was assessed *in vitro* using RAW 264.7 murine macrophages, with IK20 RPM as a control. Cells were incubated with increasing concentrations of each RPM for 24 hours, and viability was measured using the MTT assay (Figure S3). The control 10-mer and 20-mer IK RPMs exhibited no cytotoxicity at concentrations up to 400 µg/ml, whereas FK20 RPM showed minimal cytotoxicity at 200 µg/ml, a concentration effective against *C. auris*. At 400 µg/ml, twice its MIC, FK20 RPM was cytotoxic to macrophages, unlike IK20 and IK10 RPMs, suggesting greater susceptibility of fungal cells to FK20's cytotoxic effect. To confirm FK20's safety *in vivo*, mice received daily intramuscular injections of FK20 RPM 25 mg/kg, IK20 RPM (25 mg/kg, control), or ultra-pure water (UPW) for four days. This dose was previously established as efficacious against drug-resistant bacteria, safe, and capable of ensuring effective drug distribution and stability throughout treatment (33). On day four, blood chemistry and hemolysis were analyzed (Figure S4, Table S1). No significant differences were observed in hemolysis or blood chemistry profiles between FK20-treated and IK10 or UPW-treated cohorts, indicating FK20's safety for therapeutic use.

To evaluate the *in vivo* efficacy of FK20 RPM, a neutropenic mouse model of invasive candidiasis was employed, involving intravenous *C. auris* challenge and assessment of treatment response via kidney fungal burden (52). Immunosuppression was induced with cyclophosphamide, followed by intravenous *C. auris* infection. Mice received daily intra-muscular injections of FK20 RPM (25 mg/kg), or IK20 RPM (25 mg/kg, control), which lacks antifungal activity. Eight days post infection, disease severity, survival, weight loss, and kidney fungal burden were assessed (Figure 8B-E). Compared to IK20-treated mice, FK20-treated mice exhibited significantly reduced clinical scores, increased survival rates, attenuated weight loss, and lower fungal burden. These findings demonstrate that FK20 RPM effectively mitigates acute *C. auris* infection *in vivo*, highlighting its therapeutic potential for systemic candidiasis.

Discussion

The escalating threat of antimicrobial resistance, underscored by reports from the World Health Organization and the CDC, represents a global public health crisis (53, 54). While *C albicans* remains prevalent, the rise of non-*albicans Candida* species, particularly multidrug-resistant *C. auris*, has shifted the epidemiology of candidiasis over the past decade, with *C. auris* classified as an urgent threat by the CDC due to high treatment failure rates (22). Current antifungals, including echinocandins, amphotericin B, and azoles, are limited by narrow spectra, toxicity, pharmacokinetic variability, and drug interactions. Echinocandins, despite favorable safety profiles, are susceptible to resistance in *C. auris*, while amphotericin B and azoles are constrained by toxicity and drug-drug interactions, respectively (55–57). These limitations, coupled with emerging resistance, necessitate novel antifungal agents with unique mechanisms and robust resistance profiles.

Our study demonstrates that FK20 RPM, a homochiral L-phenylalanine–L-lysine 20-mer, exhibits superior antifungal activity against *C. auris* compared to other RPMs, including heterochiral and compositional variants. Our analysis revealed extensive FK20 RPM-induced cell wall and cell membrane damage as judged by visualization of FK20's internalization into *C. auris* cells, scanning electron microscopy (SEM) showing FK20 RPM-induced surface damage, propidium iodide (PI) staining confirming concentration-dependent membrane damage, induction of ROS, and membrane depolarization (Figure 5), all supporting the observed effects on *C. auris* outer surface integrity. *In vitro* experimental evolution revealed *C. auris's* inability to develop resistance to FK20, with no change in MIC_{50} after ten passages, in stark contrast to rapid caspofungin resistance (>10 µg/ml MIC_{50} increase) (Figure 6B-C). Notably, caspofungin-resistant strains exhibited collateral sensitivity to FK20, with reduced MIC_{50}, while FK20-exposed strains maintained caspofungin susceptibility (Figure 6D-E). The collateral sensitivity of caspofungin-resistant *C. auris* to FK20, combined with their synergistic interaction (FICI 0.378, Figure 7A), positions FK20 and caspofungin as a promising combination therapy. FK20's disruption of cell walls and membranes complements caspofungin inhibition of (1→3)-β-D-glucan synthase, leading to enhanced cell wall damage and osmotic stress. This synergy enabled complete biofilm inhibition at concentrations 32-fold and 15-fold lower than the individual MICs of FK20 and caspofungin, respectively (Figure 7B–C), addressing *C. auris*'s biofilm-mediated resistance, which limits caspofungin alone (>32 µg/ml for 90% inhibition). Crucially, combination therapy may forestall caspofungin resistance development. As *C. auris* evolves resistance to caspofungin, it becomes more susceptible to FK20, ensuring fungal eradication during co-treatment and reducing the likelihood of resistance emergence. This evolutionary trade-off, where resistance to one drug enhances susceptibility to another, mirrors strategies in antibacterial combination therapies and offers a novel approach to combat *C. auris*'s rapid resistance profile.

FK20's therapeutic potential is further supported by its safety and efficacy. *In vitro* FK20 exhibited minimal cytotoxicity to RAW 264.7 macrophages at 200 µg/ml, sufficient for *C. auris* treatment, unlike cytotoxic effects at 400 µg/ml, suggesting fungal-specific activity (Figure S3). *In vivo*, FK20 (25 mg/kg) showed no adverse effects on blood chemistry and hemolysis in mice (Figure S4, Table S1), supporting its overall safety profile. In a neutropenic mouse model of candidiasis, FK20 significantly reduced fungal burden, clinical scores, and weight loss, and increased survival compared to IK20-treated controls (Figure 8B–E), confirming its efficacy against systemic infection.

Beyond *C. auris*, FK20's in vitro activity against other *Candida* species (e.g., *C. albicans*, *C. glabrata*, *C. parapsilosis*) suggests broader therapeutic applications (Figure 2). This broad-spectrum potential, coupled with its resistance evasion and synergy with caspofungin, positions FK20 as a versatile antifungal candidate. The synergy and collateral sensitivity with caspofungin warrant further investigation in vivo, as our current data are limited to *C. auris* models, to confirm resistance suppression and efficacy across *Candida* species.

In conclusion, FK20 RPM offers a novel antifungal strategy against *C. auris* through its potent cell surface damage, resistance evasion, and synergistic potential with caspofungin. Its ability to exploit collateral sensitivity in caspofungin-resistant strains enhances its promise for combination therapy, potentially mitigating *C. auris*'s rapid resistance development. These attributes, alongside its safety and efficacy *in vitro* and *in vivo*, underscore FK20's potential as a transformative therapeutic for systemic candidiasis, with broader applications pending further clinical development.

ACKNOWLEDGMENTS

Funding

This work was funded by Israeli Science Foundation (ISF) grants 3021/20 and 1760/20.

Author contributions

Conceptualization: JA, YB, ZH, and NS

Investigation: JA, YB, MR, HH, AI, ZH, and NS.

Funding acquisition: ZH and NS

Supervision: ZH and NS

Writing: JA, YB, ZH, and NS

Materials and Methods

Peptide Synthesis

Peptides were synthesized by a standard Fmoc-based solid-phase peptide synthesis (SPPS) on Rink Amide resin (substitution 0.6 mmol/gr), using a peptide synthesizer (Liberty Blue). Amino acids were diluted with dimethylformamide (DMF) to a final concentration of 0.2 M. Before coupling execution, 4 equivalents of amino acids were activated in DMF using 4 equiv. of DIC and 8 equiv. Oxyma. Fmoc deprotection was conducted by 20% piperidine in DMF. At the end of the synthesis, the peptide mixtures were cleaved from the resin by adding a solution containing 95% trifluoroacetic acid (TFA), 2.5% double-distilled water (DDW) and 2.5% triisopropylsilane (TIPS) and stirred for 3 hours. The mixture was then filtered, and the peptides precipitated by the addition of 40 ml cold diethyl ether to the TFA solution and centrifuged. The supernatant was then removed and the peptide pellet dried, dissolved in 20% acetonitrile in DDW, frozen with liquid nitrogen and lyophilized. The synthesis was validated by MALDI-TOF mass spectrometry.

Cells and Reagents

Mouse macrophage-like RAW 264.7 cells were cultured in DMEM medium supplemented with 10% fetal bovine serum, 1% glutamine, 100 units/ml penicillin/streptomycin and maintained at 37°C in 5% CO_2. Toxicity assay was done using 3-(4, 5,-dimethyl thiazolyl-2)-2,5-diphenyl tetrazolium bromide assay (MTT).

C. auris Killing Assay

Overnight starter of *C. auris* was prepared in 5ml of YPD media, and grew at 37°C, 200 rpm. The starter was washed three times with PBS. Cells were counted using haemocytometer and resuspended in PBS. 10^6 cells/ml were incubated with 50 or 200 µg/ml of each RPM separately for 45 min at 37°C, 200 RPM in PBS. The microbial burden was calculated after dilutions and plating each sample on YPD agar plates.

Mice, Animal Care, and Ethics Statement

All experiments involving the use of mice were approved by and performed according to the Hebrew University of Jerusalem Institutional Animal Care and Use Committee (IACUC) (protocol number MD-21-16494-5). The Hebrew University of Jerusalem is accredited by the NIH and by AAALAC to perform experiments on laboratory animals (NIH approval number: OPRR-A01-5011). Eight-week-old C57BL/6JOlaHsd female mice (18-20g) mice were purchased from Envigo, Israel. Mice were housed under specific pathogen-free conditions in groups of five in individually ventilated cages with unrestricted access to food and water.

Murine Model of Systemic Candidiasis

Mice were immunosuppressed by intra-peritoneal injection of 0.2ml cyclophosphamide in PBS at a concentration of 150 mg/kg three days before infection, followed by 100mg/kg one day before infection, and two days post-infection. Subsequent injection of cyclophosphamide (100mg/kg) were administered at two-day intervals following infection in the survival experiment. Infection inoculum was obtained by sub-culturing *Candida auris* on agar plates grown at 37°C for 24h. Single colonies of *C. auris* were resuspended in PBS and adjusted to specified concentrations. Immunosuppressed mice were infected with 1 x 10^6 CFUs in 0.1 ml of PBS *via* the lateral tail vein injection. Treatment of mice with 25 µg/gr body weight of each RPM was initiated approximately 2 hours after infection and repeated daily throughout the course of the experiment. Following infection, the health status and survival of mice were monitored daily. Clinical scores were assigned to each mouse to evaluate disease severity using disease severity indices obtained from observations of mice activity, grooming, lethargy, and posture. Mice showing severe signs of disease were humanely euthanized. The survival curves were analyzed by log-rank (Mantel-Cox) test using GraphPad Prism software version 8.00 (GraphPad Software, USA). Mice were sacrificed and the excised kidneys were weighed followed by homogenization using GentleMACS Dissociator (Miltenyi Biotec). Subsequently, 100 µL of the organ homogenate was used in the determination of CFUs following a 1:10000 dilution.

Determination of MIC

Minimum Inhibitory Concentration (MIC) assays for *C. auris* B11117 strains were performed for FK20 and caspofungin according to European Committee on Antibiotic Susceptibility Testing (EUCAST) guidelines for determination of MIC using broth microdilution method (58), (59). Single colonies were obtained for *Candida auris* B1117 strains streaked on Sabouraud Dextrose Agar (40 gr/L Dextrose, 10 gr/L Peptone, at pH 5.6) plates at 37°C for 24h. Approximately 1 x 10^5 *C. auris* cells were incubated in 200ul filter sterilized RPMI-1640 culture media (Sigma), supplemented with 1.8% glucose to reach a final concentration of 2% and 0.03% L-Glutamine at pH 7.0. The growth media was supplemented with serial dilutions of antifungal agents 0 to 400 µg/ml of FK20 RPM, and 0 to 64 µg/ml of caspofungin in different 96-well microtiter plates. Cells were incubated in 96-well microtiter plates at 37°C and MIC was determined spectrophotometrically after 28h, 48h, and 72h using Tecan Infinite M Plex plate reader (Neotec Bio, Israel).

Drug Combination Assay and Determination of Fractional Inhibitory Concentration

The combined efficacy of Caspofungin and FK20 was determined *in vitro* using a checkerboard assay, followed by the calculation of the Fractional Inhibitory Concentration Index (FICI). Caspofungin and FK20 were added individually at a volume of 50 µL per well in four-fold strength, yielding a final concentration of 0-3.2 µg/ml for Caspofungin and 0-2000 to 200 µg/ml for FK20. The yeast inoculum (1 x 10^5 cells per well) was added to the plates. Plates were then incubated at 37°C for a duration of

72 hours. The antifungal combination activities of caspofungin and FK20 were assessed based on their FICI. The FICI was derived from the Minimum Inhibitory Concentration (MIC-50), representing the inhibitory concentration at which 50% of the cell population are killed by the effect of the drug combination. The FICI was determined by the formula; $index = FIC_A + FIC_B = \frac{[A]}{MIC_A} + \frac{[B]}{MIC_B}$, where [A] and [B] are concentrations of drugs A and B, and MIC_A and MIC_B are their respective MIC values for *C. auris*. Results were interpreted as follows: Synergy (FICI ≤ 0.5), partial synergy (0.5 < FICI ≤ 0.75), additive (0.75 < FICI ≤ 1), indifferent (1 < FICI ≤ 4), and antagonistic (FICI > 4).

Biofilm Formation and Quantification

In a 96-well microtiter plate, 200 µL of *C. auris* cells at a concentration of 10^6 CFU/ ml were cultured in RPMI-1640 medium, supplemented with L-Glutamine (1%) and glucose (2%) for 24 hours at 37ºC together with different concentrations of a FK20, caspofungin, or combinations that were tested to study their effects on biofilm formation. Inhibition of biofilm formation was assessed using a crystal violet assay. Planktonic cells were removed, mature biofilms were washed with DDW and then stained with 125 µL of 0.1% crystal violet for 15 minutes. Excess stain was washed off, and the biofilms were air-dried for 4 hours at 25ºC. Finally, they were re-stained with 125 µL of 30% acetic acid and biofilm biomass was quantified at 595 nm using a microplate reader (Tecan infinite M200). Biofilm formation was also assessed using the 3-(4,5-dimethylthiazol-2)-2,5-diphenyltetrazolium bromide (MTT) assay. In this method, each well was loaded with 50 µL of MTT reagent (1.5 mg/ml), and the plate was incubated for 1.5 hours at 37ºC. Subsequently, 150 µL of dimethyl sulfoxide (DMSO) was added, and the plate was incubated for 10 minutes at 30ºC with agitation at 180 RPM. The absorbance was then measured at 595 nm using a TECAN Infinite plate reader.

***In vitro* experimental evolution**

In vitro experimental evolution of *Candida auris* was performed according to the protocol published in (45) with minor modifications. Briefly, *C. auris* B11117 was independently passaged through 100 µg/ml of FK20 RPM and 2 µg/ml of caspofungin. *C. auris* was also passaged simultaneously without exposure to any antifungal drug. The concentration of FK20 RPM selected for the experimental evolution was equivalent to the predetermined MIC_{50} of the parental *C. auris* B11117 strain. The experimental evolution was initiated by generating three independent replicates of *C. auris* B11117 as the parental strain. Cultures were struck from frozen parental stocks onto Sabouraud Dextrose Agar (40 gr/L Dextrose, 10 gr/L Peptone, at pH 5.6) plates and incubated at 37°C overnight. Each parental replicate was generated from randomly selected single colonies. Subcultures were made in YPD liquid media and incubated at 37°C overnight at 100 rpm. The overnight culture was diluted 1:1000 in RPMI-1640 (supplemented with 1.8% glucose to reach a final concentration of 2% glucose and 0.03% L-Glutamine at pH 7.0) to a final volume of 1ml. RPMI-1640 media was supplemented with

100µg/ml of FK20 and 2.5 µg/ml of caspofungin for replicates evolved with FK20 and caspofungin respectively, and supplemented RPMI-1640 media for replicates evolved without drugs in 96-deep well plates and incubated at 37°C for 72 hr. From cultures of each replicate, 100 µL of each replicate was frozen in 25% glycerol as parental replicates at time zero. Precautions were taken to minimize contaminations while keeping environmental conditions similar. Plates were sealed with gas-permeable membranes to allow gas exchange and maximum growth. The 96-deep well plate was incubated at 37°C without shaking to mimic static growth used in clinical resistance assays. Plates were incubated in plastic trays lined with wet paper towels to minimize evaporation. Following incubation for 72 hr, individual wells were mixed by pipetting and diluted 1:10 into fresh RPMI-1640 supplemented with or without drugs. In total 10 transfers were carried out, and 100 µL of evolved replicate cultures were frozen in duplicates in 25% glycerol for each transfer until after the tenth transfer and maintained at -80°C.

Determination of Resistance for Evolved Strains

Initial susceptibility of all parental strains was tested using broth microdilution liquid assays to determine the MIC_{50} that is, the concentration of antifungal agent at which 50 percent of the cell population are eliminated. The liquid assay experiment was carried out according to cell dilution regulations of the European Committee on Antibiotic Susceptibility Testing (EUCAST) guidelines with some modifications (58), (59). Briefly, RPMI incubated at 37°C was used at the base media, and growth was determined as absorbance of cell densities at OD_{590} at 24, 48, and 72 hr post-inoculation. MIC_{50} was numerically calculated as the concentration in which a 50% decrease in turbidity was determined spectrophotometrically.

Viability Staining

To assess the fungicidal activity of FK20, approximately 1 x 10^6 cells/ml were incubated with varying concentrations of FK20, ranging from 0 to 400 µg/ml for 45 minutes at 37C with continuous shaking. Subsequently, treated cells were washed with PBS and resuspended with either Propidium Iodide (1:25 dilution of 0.5mg/ml, BioLegend) or Ghost-Dye (1:500 dilution, Tonbo Biosciences) viability stain for 20 minutes. Residual viability dyes were washed with PBS, and cells were resuspended in PBS for analysis of fluorescence by flow cytometer.

Reactive oxygen species (ROS) detection

Approximately 1 x 10^6 cells/ml were incubated with 200 µg/ml of FK20 for 45 minutes at 37°C with continuous shaking at 200 RPMs. Treated and untreated cells were washed with PBS and resuspended with 10µM dihydrorhodamine 123 (DHR123, Cayman Chemical) to detect intracellular ROS by staining for 20 minutes. Residual dyes were washed with PBS, and cells were resuspended in PBS for analysis of fluorescence by flow cytometer.

Cell membrane depolarisation

To test the effect of RPMs on cell membrane depolarisation of *C. auris*, 1 x 10^6 cells/ml were incubated with 200 µg/ml of FK20 for 45 minutes at 37°C with continuous shaking at 200 RPMs. Treated and untreated cells were washed with PBS and resuspended with 5µM bis-(1,3-dibutylbarbituric Acid) pentamethine oxonol ($DIBAC_4(5)$, Santa Cruz) to detect intracellular ROS by staining for 20 minutes. ells were resuspended in PBS for analysis of fluorescence by flow cytometer.

References

1. Chinemerem Nwobodo D, Ugwu MC, Oliseloke Anie C, Al-Ouqaili MTS, Chinedu Ikem J, Victor Chigozie U, Saki M. 2022. Antibiotic resistance: The challenges and some emerging strategies for tackling a global menace. J Clin Lab Anal 36:1–10.

2. Murray CJ, Ikuta KS, Sharara F, Swetschinski L, Robles Aguilar G, Gray A, Han C, Bisignano C, Rao P, Wool E, Johnson SC, Browne AJ, Chipeta MG, Fell F, Hackett S, Haines-Woodhouse G, Kashef Hamadani BH, Kumaran EAP, McManigal B, Agarwal R, Akech S, Albertson S, Amuasi J, Andrews J, Aravkin A, Ashley E, Bailey F, Baker S, Basnyat B, Bekker A, Bender R, Bethou A, Bielicki J, Boonkasidecha S, Bukosia J, Carvalheiro C, Castañeda-Orjuela C, Chansamouth V, Chaurasia S, Chiurchiù S, Chowdhury F, Cook AJ, Cooper B, Cressey TR, Criollo-Mora E, Cunningham M, Darboe S, Day NPJ, De Luca M, Dokova K, Dramowski A, Dunachie SJ, Eckmanns T, Eibach D, Emami A, Feasey N, Fisher-Pearson N, Forrest K, Garrett D, Gastmeier P, Giref AZ, Greer RC, Gupta V, Haller S, Haselbeck A, Hay SI, Holm M, Hopkins S, Iregbu KC, Jacobs J, Jarovsky D, Javanmardi F, Khorana M, Kissoon N, Kobeissi E, Kostyanev T, Krapp F, Krumkamp R, Kumar A, Kyu HH, Lim C, Limmathurotsakul D, Loftus MJ, Lunn M, Ma J, Mturi N, Munera-Huertas T, Musicha P, Mussi-Pinhata MM, Nakamura T, Nanavati R, Nangia S, Newton P, Ngoun C, Novotney A, Nwakanma D, Obiero CW, Olivas-Martinez A, Olliaro P, Ooko E, Ortiz-Brizuela E, Peleg AY, Perrone C, Plakkal N, Ponce-de-Leon A, Raad M, Ramdin T, Riddell A, Roberts T, Robotham JV, Roca A, Rudd KE, Russell N, Schnall J, Scott JAG, Shivamallappa M, Sifuentes-Osornio J, Steenkeste N, Stewardson AJ, Stoeva T, Tasak N, Thaiprakong A, Thwaites G, Turner C, Turner P, van Doorn HR, Velaphi S, Vongpradith A, Vu H, Walsh T, Waner S, Wangrangsimakul T, Wozniak T, Zheng P, Sartorius B, Lopez AD, Stergachis A, Moore C, Dolecek C, Naghavi M. 2022. Global burden of bacterial antimicrobial resistance in 2019: a systematic analysis. Lancet 399:629–655.

3. Zhang Z, Zhang Q, Wang T, Xu N, Lu T, Hong W, Penuelas J, Gillings M, Wang M, Gao W, Qian H. 2022. Assessment of global health risk of antibiotic resistance genes. Nat Commun 13.

4. Nelson RE, Hatfield KM, Wolford H, Samore MH, Scott RD, Reddy SC, Olubajo B, Paul P, Jernigan JA, Baggs J. 2021. National estimates of healthcare costs associated with multidrug-resistant bacterial infections among hospitalized patients in the United States. Clin Infect Dis 72:S17–S26.

5. Horton M V., Holt AM, Nett JE. 2023. Mechanisms of pathogenicity for the emerging fungus Candida auris. PLoS Pathog https://doi.org/10.1371/journal.ppat.1011843.

6. Cristina ML, Spagnolo AM, Sartini M, Carbone A, Oliva M, Schinca E, Boni S, Pontali E. 2023. An Overview on Candida auris in Healthcare Settings. J Fungi 9:913.

7. Centers for Disease Control and Prevention. 2019. Antibiotic Resistance Threats in The United States 2019. Antibiot Resist Threat United States (US Dep Heal Hum Serv 10.

8. Satoh K, Makimura K, Hasumi Y, Nishiyama Y, Uchida K, Yamaguchi H. 2009. Candida auris sp. nov., a novel ascomycetous yeast isolated from the external ear canal of an inpatient in a Japanese hospital. Microbiol Immunol 53:41–44.

9. Lockhart SR, Adam R, Alanio A, Alastruey-izquierdo A, Althawadi S, Araúz B. 2020. Tracing the Evolutionary History and Global Expansion of Candida auris Using Population Genomic Analyses. MBio 11.

10. Suphavilai C, Ko KKK, Lim KM, Tan MG, Boonsimma P, Chu JJK, Goh SS, Rajandran P, Lee LC, Tan KY, Shaik Ismail BB, Aung MK, Yang Y, Sim JXY, Venkatachalam I, Cherng BPZ, Spruijtenburg B, Chan KS, Oon LLE, Tan AL, Tan YE, Wijaya L, Tan BH, Ling ML, Koh TH, Meis JF, Tsui CKM, Nagarajan N. 2024. Detection and characterisation of a sixth

Candida auris clade in Singapore: a genomic and phenotypic study. The Lancet Microbe 5:100878.

11. Spruijtenburg B, Badali H, Abastabar M, Mirhendi H, Khodavaisy S, Sharifisooraki J, Taghizadeh Armaki M, de Groot T, Meis JF. 2022. Confirmation of fifth Candida auris clade by whole genome sequencing. Emerg Microbes Infect 11:2405–2411.

12. Rhodes J, Fisher MC. 2019. Global epidemiology of emerging Candida auris. Curr Opin Microbiol 52:84–89.

13. Welsh RM, Bentz ML, Shams A, Houston H, Lyons A, Rose LJ, Litvintseva AP. 2017. Survival, Persistence, and Isolation of the Emerging Multidrug-Resistant Pathogenic Yeast Candida auris on a Plastic Health Care Surface. J Clin Microbiol 55:2996–3005.

14. Lockhart SR, Etienne KA, Vallabhaneni S, Farooqi J, Chowdhary A, Govender NP, Colombo AL, Calvo B, Cuomo CA, Desjardins CA, Berkow EL, Castanheira M, Magobo RE, Jabeen K, Asghar RJ, Meis JF, Jackson B, Chiller T, Litvintseva AP. 2017. Simultaneous emergence of multidrug-resistant candida auris on 3 continents confirmed by whole-genome sequencing and epidemiological analyses. Clin Infect Dis 64:134–140.

15. Arensman K, Miller JL, Chiang A, Mai N, Levato J, LaChance E, Anderson M, Beganovic M, Dela Pena J. 2020. Clinical Outcomes of Patients Treated for Candida auris Infections in a Multisite Health System, Illinois, USA. Emerg Infect Dis 26:866–871.

16. Jangir P, Kalra S, Tanwar S, Bari VK. 2023. Azole resistance in Candida auris: mechanisms and combinatorial therapy. Apmis 131:442–462.

17. Chen J, Tian S, Han X, Chu Y, Wang Q, Zhou B, Shang H. 2020. Is the superbug fungus really so scary? A systematic review and meta-analysis of global epidemiology and mortality of Candida auris. BMC Infect Dis 20:1–10.

18. Tu J, Zhu T, Wang Q, Yang W, Huang Y, Xu D, Liu N, Sheng C. 2023. Discovery of a new chemical scaffold for the treatment of superbug Candida auris infections. Emerg Microbes Infect 12.

19. Chowdhary A, Prakash A, Sharma C, Kordalewska M, Kumar A, Sarma S, Tarai B, Singh A, Upadhyaya G, Upadhyay S, Yadav P, Singh PK, Khillan V, Sachdeva N, Perlin DS, Meis JF. 2018. A multicentre study of antifungal susceptibility patterns among 350 Candida auris isolates (2009-17) in India: Role of the ERG11 and FKS1 genes in azole and echinocandin resistance. J Antimicrob Chemother 73:891–899.

20. Chaabane F, Graf A, Jequier L, Coste AT. 2019. Review on Antifungal Resistance Mechanisms in the Emerging Pathogen Candida auris. Front Microbiol 10:1–8.

21. Sanyaolu A, Okorie C, Marinkovic A, Abbasi AF, Prakash S, Mangat J, Hosein Z, Haider N, Chan J. 2022. Candida auris: An Overview of the Emerging Drug-Resistant Fungal Infection. Infect Chemother 54:236–246.

22. Chowdhary A, Voss A, Meis JF. 2016. Multidrug-resistant Candida auris : ‘new kid on the block’ in hospital-associated infections? J Hosp Infect 94:209–212.

23. Hu S, Zhu F, Jiang W, Wang Y, Quan Y, Zhang G, Gu F, Yang Y. 2021. Retrospective Analysis of the Clinical Characteristics of Candida auris Infection Worldwide From 2009 to 2020. Front Microbiol 12:1–9.

24. Geremia N, Brugnaro P, Solinas M, Scarparo C, Panese S. 2023. Candida auris as an Emergent Public Health Problem: A Current Update on European Outbreaks and Cases. Healthc 11:1–12.

25. Chowdhary A, Anil Kumar V, Sharma C, Prakash A, Agarwal K, Babu R, Dinesh KR, Karim

S, Singh SK, Hagen F, Meis JF. 2014. Multidrug-resistant endemic clonal strain of Candida auris in India. Eur J Clin Microbiol Infect Dis 33:919–926.

26. Arendrup MC, Prakash A, Metetiadis J, Sharma C, Chowdhary A. 2017. Comparison of EUCAST and CLSI Reference Microdilution MICs of Eight and Associated Tentative. Antimicrob Agents Chemother 61:1–10.

27. Huan Y, Kong Q, Mou H, Yi H. 2020. Antimicrobial Peptides: Classification, Design, Application and Research Progress in Multiple Fields. Front Microbiol 11:1–21.

28. Ageitos JM, Sánchez-Pérez A, Calo-Mata P, Villa TG. 2017. Antimicrobial peptides (AMPs): Ancient compounds that represent novel weapons in the fight against bacteria. Biochem Pharmacol 133:117–138.

29. Kumar P, Kizhakkedathu JN, Straus SK. 2018. Antimicrobial peptides: Diversity, mechanism of action and strategies to improve the activity and biocompatibility in vivo. Biomolecules 8.

30. Reddick LE, Alto NM. 2014. Bacteria fighting back: How pathogens target and subvert the host innate immune system. Mol Cell 54:321–328.

31. Amso Z, Hayouka Z. 2019. Antimicrobial random peptide cocktails: A new approach to fight pathogenic bacteria. Chem Commun 55:2007–2014.

32. Stern T, Zelinger E, Hayouka Z. 2016. Random peptide mixtures inhibit and eradicate methicillin-resistant: Staphylococcus aureus biofilms. Chem Commun 52:7102–7105.

33. Bennett RC, Oh MW, Kuo SH, Belo Y, Maron B, Malach E, Lin J, Hayouka Z, Lau GW. 2021. Random Peptide Mixtures as Safe and Effective Antimicrobials against Pseudomonas aeruginosa and MRSA in Mouse Models of Bacteremia and Pneumonia. ACS Infect Dis 7:672–680.

34. Topman S, Tamir-Ariel D, Bochnic-Tamir H, Stern Bauer T, Shafir S, Burdman S, Hayouka Z. 2018. Random peptide mixtures as new crop protection agents. Microb Biotechnol 11:1027–1036.

35. Lau JZ, Kuo SH, Belo Y, Malach E, Maron B, Caraway HE, Oh MW, Zhang Y, Ismail N, Lau GW, Hayouka Z. 2023. Antibacterial efficacy of an ultra-short palmitoylated random peptide mixture in mouse models of infection by carbapenem-resistant Klebsiella pneumoniae . Antimicrob Agents Chemother 67:1–18.

36. Cheriker H, Stern Bauer T, Oren Y, Nir S, Hayouka Z. 2020. Immobilized random peptide mixtures exhibit broad antimicrobial activity with high selectivity. Chem Commun 56:11022–11025.

37. Hayouka Z, Chakraborty S, Liu R, Boersma MD, Weisblum B, Gellman SH. 2013. Interplay among subunit identity, subunit proportion, chain length, and stereochemistry in the activity profile of sequence-random peptide mixtures. J Am Chem Soc 135:11748–11751.

38. Topman-Rakover S, Malach E, Burdman S, Hayouka Z. 2020. Antibacterial lipo-random peptide mixtures exhibit high selectivity and synergistic interactions. Chem Commun 56:12053–12056.

39. Rosenberg M, Azevedo NF, Ivask A. 2019. Propidium iodide staining underestimates viability of adherent bacterial cells. Sci Rep 9:1–12.

40. Stiefel P, Schmidt-Emrich S, Maniura-Weber K, Ren Q. 2015. Critical aspects of using bacterial cell viability assays with the fluorophores SYTO9 and propidium iodide. BMC Microbiol 15:1–9.

41. Cho J, Lee DG. 2011. The antimicrobial peptide arenicin-1 promotes generation of reactive oxygen species and induction of apoptosis. Biochim Biophys Acta - Gen Subj 1810:1246–

1251.

42. Wenzel M, Chiriac AI, Otto A, Zweytick D, May C, Schumacher C, Gust R, Albada HB, Penkova M, Krämer U, Erdmann R, Metzler-Nolte N, Straus SK, Bremer E, Becher D, Brötz-Oesterhelt H, Sahl H-G, Bandow JE. 2014. Small cationic antimicrobial peptides delocalize peripheral membrane proteins. Proc Natl Acad Sci 111:1409–1418.

43. Yakir I, Cohen E, Schlesinger S, Hayouka Z. 2025. Random antimicrobial peptide mixtures as non-antibiotic antimicrobial agents for cultured meat industry. Food Chem Mol Sci 10:100240.

44. Maron B, Rolff J, Friedman J, Hayouka Z. 2022. Antimicrobial Peptide Combination Can Hinder Resistance Evolution. Microbiol Spectr 10.

45. Gerstein AC, Berman J. 2020. Candida albicans Genetic Background Influences Mean and Heterogeneity of Drug Responses and Genome Stability during Evolution in Fluconazole. mSphere 5.

46. Yekani M, Azargun R, Sharifi S, Nabizadeh E, Nahand JS, Ansari NK, Memar MY, Soki J. 2023. Collateral sensitivity: An evolutionary trade-off between antibiotic resistance mechanisms, attractive for dealing with drug-resistance crisis. Heal Sci Reports 6:1–10.

47. Munck C, Gumpert HK, Wallin AIN, Wang HH, Sommer MOA. 2014. Prediction of resistance development against drug combinations by collateral responses to component drugs. Sci Transl Med 6.

48. Lara-Aguilar V, Rueda C, García-Barbazán I, Varona S, Monzón S, Jiménez P, Cuesta I, Zaballos Á, Zaragoza Ó. 2021. Adaptation of the emerging pathogenic yeast Candida auris to high caspofungin concentrations correlates with cell wall changes. Virulence 12:1400–1417.

49. Mun SH, Joung DK, Kim YS, Kang OH, Kim SB, Seo YS, Kim YC, Lee DS, Shin DW, Kweon KT, Kwon DY. 2013. Synergistic antibacterial effect of curcumin against methicillin-resistant Staphylococcus aureus. Phytomedicine 20:714–718.

50. Sherry L, Ramage G, Kean R, Borman A, Johnson EM, Richardson MD, Rautemaa-Richardson R. 2017. Biofilm-Forming Capability of Highly Virulent, Multidrug-Resistant Candida auris. Emerg Infect Dis 23:328–331.

51. Romera D, Aguilera-Correa JJ, Gadea I, Viñuela-Sandoval L, García-Rodríguez J, Esteban J. 2019. Candida auris: a comparison between planktonic and biofilm susceptibility to antifungal drugs. J Med Microbiol 68:1353–1358.

52. Zhao M, Lepak AJ, VanScoy B, Bader JC, Marchillo K, Vanhecker J, Ambrose PG, Andes DR. 2018. In Vivo Pharmacokinetics and Pharmacodynamics of APX001 against Candida spp. in a Neutropenic Disseminated Candidiasis Mouse Model. Antimicrob Agents Chemother 62.

53. CDC. 2019. Antibiotic resistance threats in the United States.US Department of Health and Human Services: Washington, DC, USA.

54. World Health Organization. 2014. Antimicrobial resistance: global report on surveillance 2014.World Health Organization, Geneva, Switzerland.

55. Gupta AK, Versteeg SG, Shear NH. 2018. Common drug-drug interactions in antifungal treatments for superficial fungal infections. Expert Opin Drug Metab Toxicol 14:387–398.

56. Kordalewska M, Lee A, Park S, Berrio I, Chowdhary A, Zhao Y, Perlin DS. 2018. Understanding Echinocandin Resistance in the Emerging Pathogen Candida auris. Antimicrob Agents Chemother 62.

57. Laniado-Laborín R, Cabrales-Vargas MN. 2009. Amphotericin B: side effects and toxicity. Rev Iberoam Micol 26:223–227.

58. Cuenca-Estrella M, Moore CB, Barchiesi F, Bille J, Chryssanthou E, Denning DW, Donnelly JP, Dromer F, Dupont B, Rex JH, Richardson MD, Sancak B, Verweij PE, Rodríguez-Tudela JL. 2003. Multicenter evaluation of the reproducibility of the proposed antifungal susceptibility testing method for fermentative yeasts of the Antifungal Susceptibility Testing Subcommittee of the European Committee on Antimicrobial Susceptibility Testing (AFST-EU. Clin Microbiol Infect 9:467–474.

59. Rodriguez-Tudela JL, Arendrup MC, Barchiesi F, Bille J, Chryssanthou E, Cuenca-Estrella M, Dannaoui E, Denning DW, Donnelly JP, Dromer F, Fegeler W, Lass-Flörl C, Moore C, Richardson M, Sandven P, Velegraki A, Verweij P. 2008. EUCAST Definitive Document EDef 7.1: method for the determination of broth dilution MICs of antifungal agents for fermentative yeasts. Clin Microbiol Infect 14:398–405.

Figures

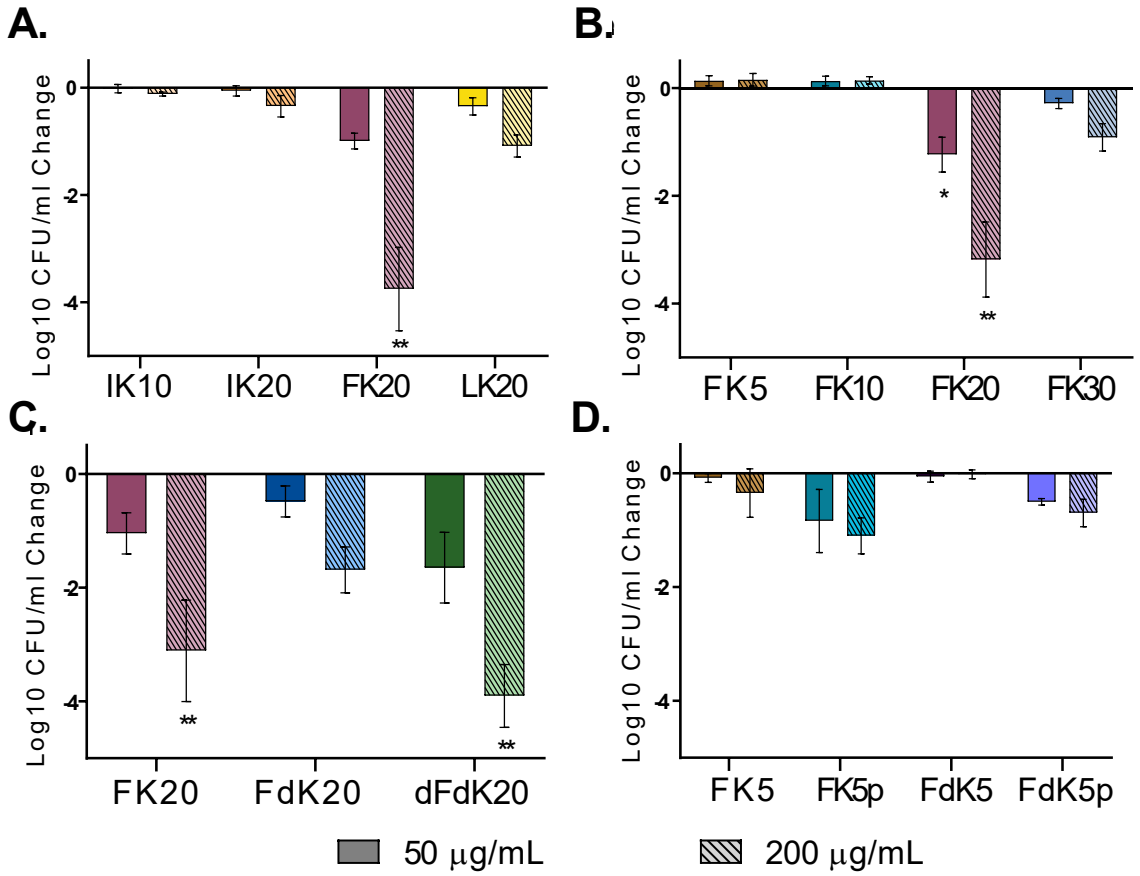

Figure 1: FK RPMs exhibit high antifungal activity against *C. auris*. *C. auris* cells were incubated with 50 or 200 μg/ml of each RPM separately for 45 min at 37°C, 200 RPM in PBS. Fungal viability was calculated by plating on YPD agar plates for CFUs. Fungicidal activity was assessed on the basis of **A.** amino acid composition (IK10, IK20, FK20 and LK20), **B.** chain length (5, 10, 20, and 30-mer FK), **C.** Stereochemistry (FK20, FdK20, and dFdK20), **D.** palmitic acid moiety addition (FK5, FK5 conjugated to palmitic acid, FdK5 and FdK5 conjugated to palmitic acid). The data are presented as average of three biologically independent experiments. Statistical significance was determined with ANOVA and Bonferroni post hoc test. *$p < 0.05$; **$p < 0.01$ significance compared to control; data without symbols are not significantly different.

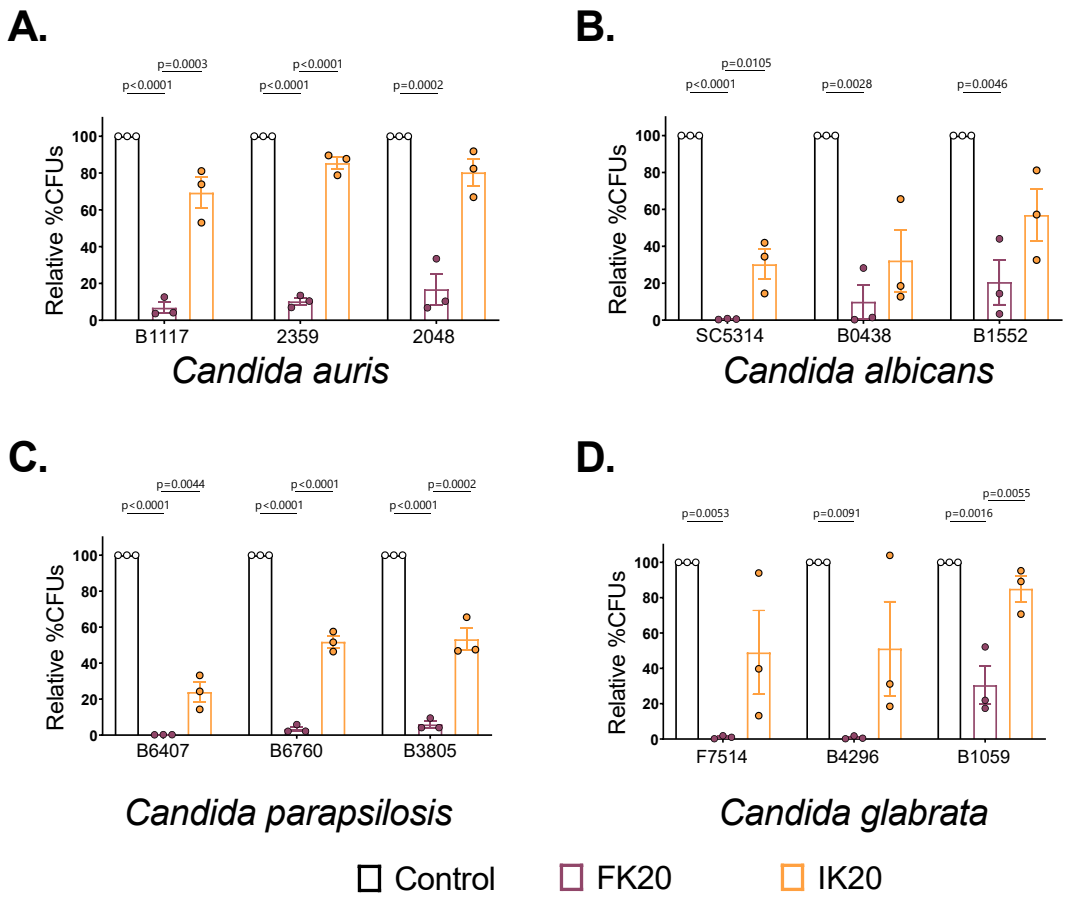

Figure 2: FK20 potency is conserved across diverse *Candida* species of clinical relevance. Cells of *C. auris* **(A.),** *C. albicans***(B.),** *C. parapsillosis* **(C.),** and *C. glabrata* **(D.)** were treated with either 200µg/ml FK20, IK20 RPMs or PBS as a control for 45 min at 37°C and analyzed for CFUs. Clinical isolates for each species include *C. auris* skin-derived isolates (1117, 2359, 2048), *C. albicans* blood-derived reference strain (SC5314) and isolates (B0438, B1552), *C. parapsillosis* blood-derived isolates (B6407, B6760, B3805), and *C. glabrata* peritoneal fluid-derived isolate (F7514) and blood-derived isolates (B4296, B1059). Data are presented as mean (SEM) of three independent biological repeats. Statistical significance was determined with One-way ANOVA with Tukey's multiple comparisons test.

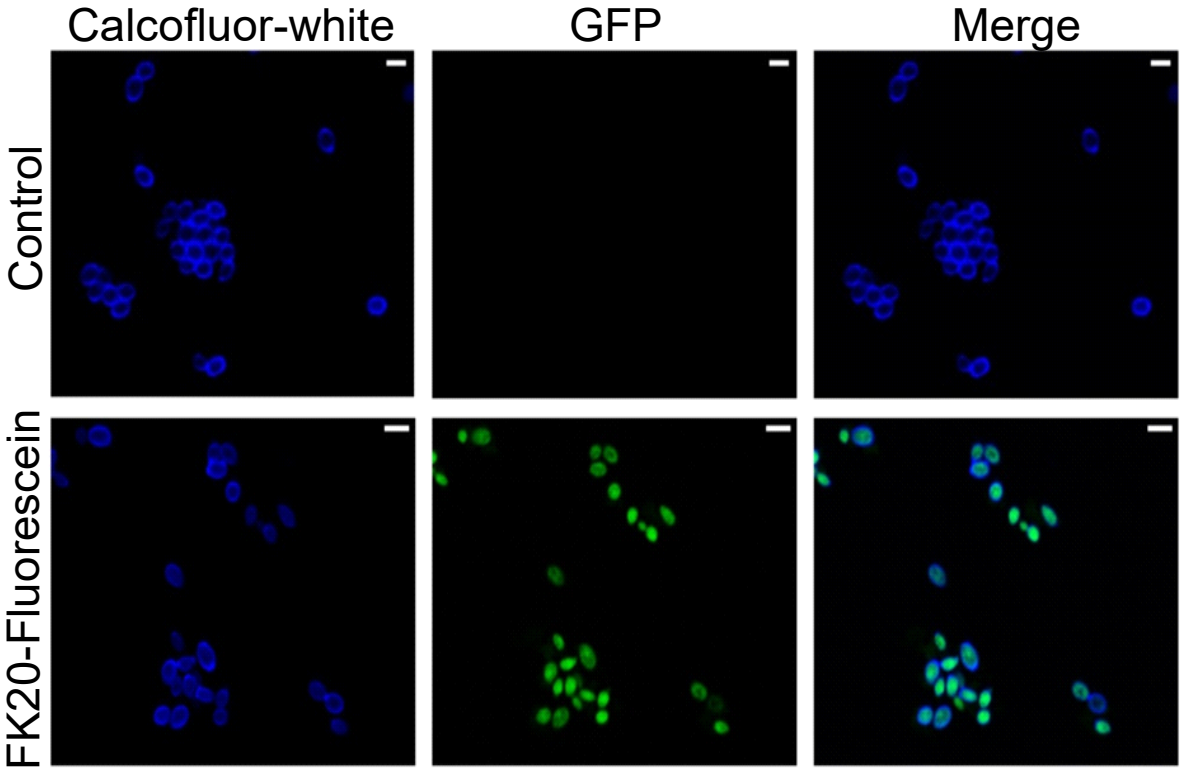

Figure 3: FK20 RPM penetrate *C. auris* cells. 5 x 10^7 CFU/ml of *C. auris* cells were incubated together with 200 µg/ml fluorescently labeled 20-mer FK RPM conjugated with fluorescein (green) for 45 min at 37ºC in PBS. Samples were stained with Calcofluor-white (blue). Images shown were taken by confocal microscope, at a magnification of 40×. Scale bars, 5µm. Images are representative of three biologically independent experiments.

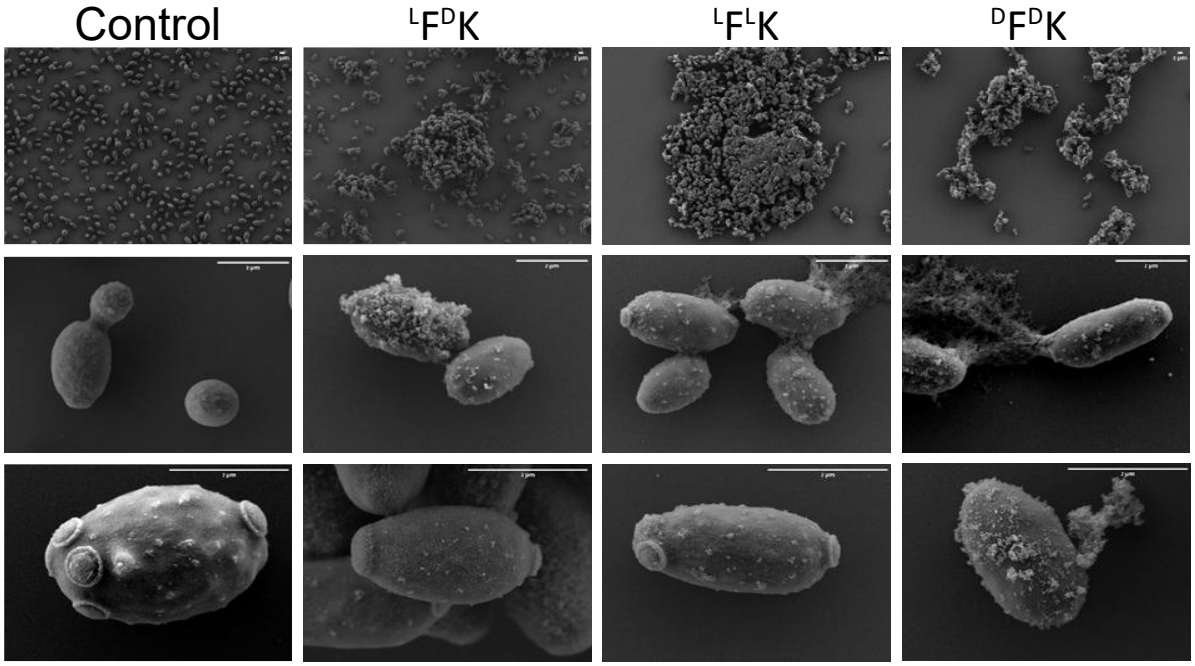

Figure 4: *C. auris* outer surface after interaction with 20-mer FK RPMs. Scanning electron microscope images depict *C. auris* untreated and treated (200 µg/ml) 20-mer FK, FdK or dFdK 1:1. The images were captured using a JEOL JSM-7800f scanning electron microscope at 20 kV. Scale bars represent 1µm. Micrographs are representative of three biologically independent experiments.

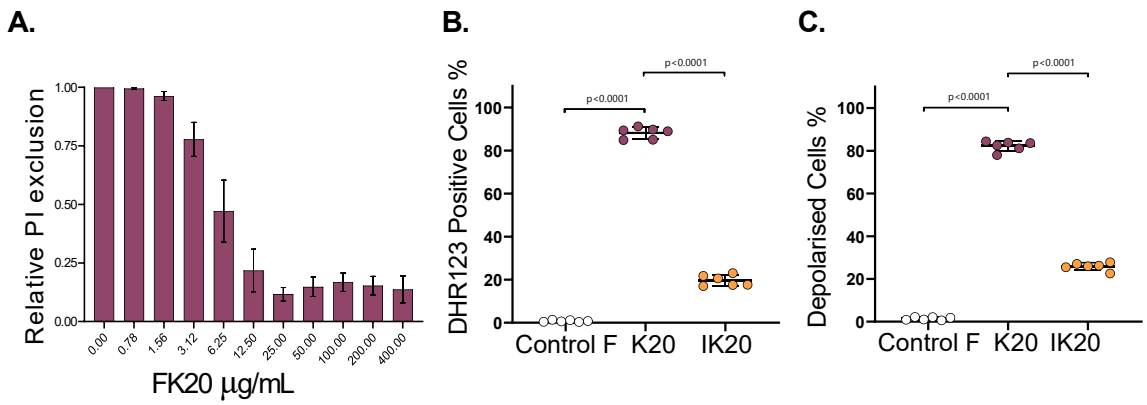

Figure 5: FK20 induces dose-dependent membrane damage, intracellular ROS production and membrane depolarization in *C. auris*. *C. auris* cells (1 x 10^6 cells) were incubated with 20-mer FK RPM at specified concentrations for 45 minutes at 37°C , 200 RPM in PBS. **A.** Membrane damage was evaluated by staining *C. auris* cells with Propidium Iodide for 20 minutes. PI uptake was determined by measuring PI fluorescence using a flow cytometer. The relative PI exclusion of *C. auris* was calculated as the percentage of cells that remained unstained by PI in treated samples relative to untreated control. The data are derived from three biologically independent experiments conducted in triplicates. **B.** ROS levels indicated as percentage DHR123 positive cells in PBS (control), FK20, and IK20 treated cells. **C.** Percentage of depolarized cells in PBS (control), FK20, and IK20 treated cells. Results shown for **(B.)** and **(C.)** are presented as mean (SEM) of two biological repetitions including three technical repetitions each. Statistical significance was determined with one-way ANOVA and Turkey's multiple comparisons test.

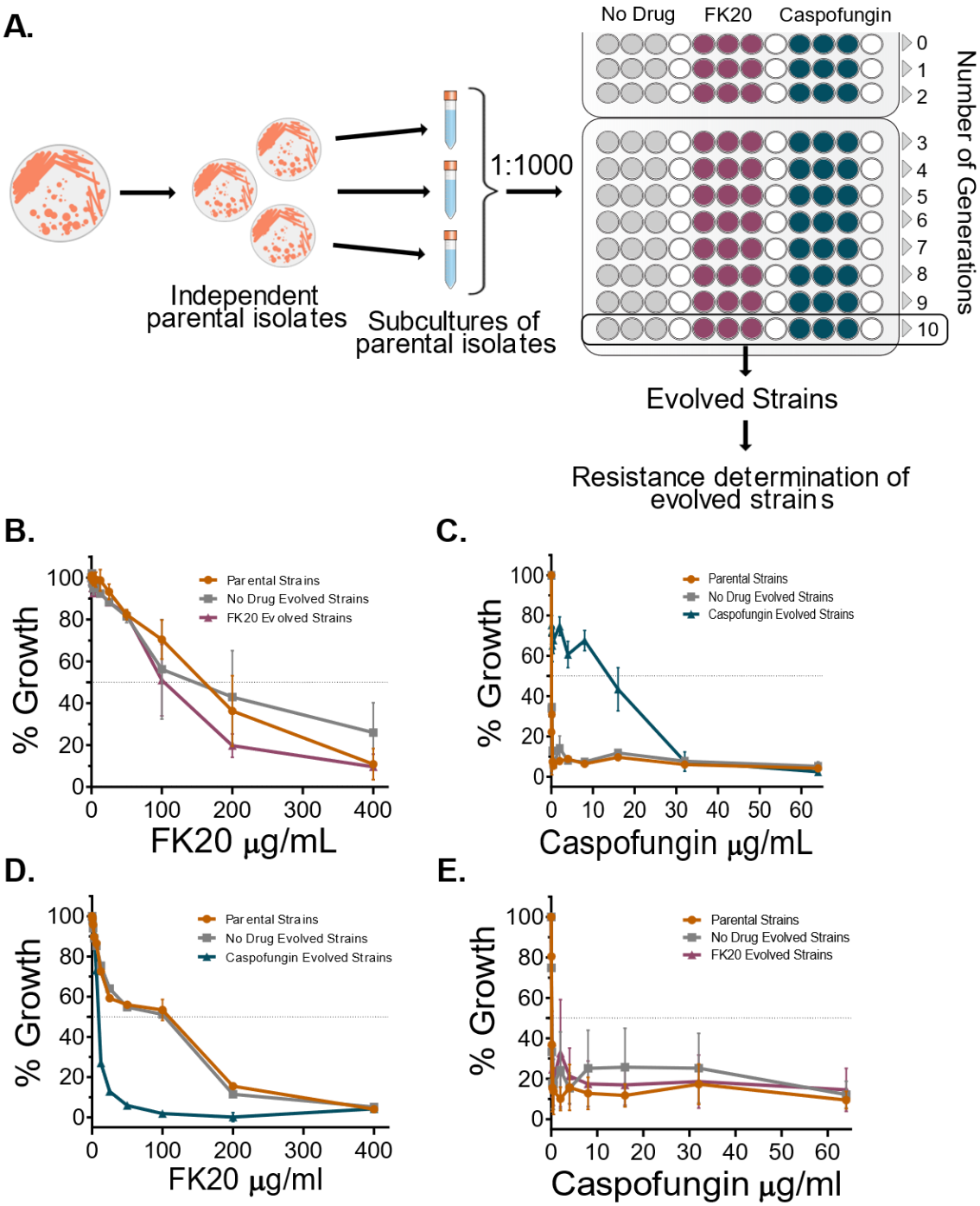

Figure 6: *In vitro*-experimental evolution. A. A scheme of experimental evolution approach of untreated or treated (FK20 or caspofungin) *C. auris*. The experimental evolution of *C. auris* was conducted with three independent replicates as initial parental strains to generate three independent evolved lineages after 10 passages. The growth profiles of the resulting strains were assessed and resistance determined by the MIC-50 values for the parental strains, non-drug-evolved strains, and strains evolved under FK20 or caspofungin conditions. The MIC was determined using the broth microdilution method after 72 hours of incubation of *C. auris* in their respective drug environments. Growth was evaluated by measuring optical density (OD590) in the presence of incrementally increasing concentrations of either FK20 **(B.)** or caspofungin **(C.)**. The percentage of growth was calculated by comparing the growth of treated *C. auris* cells to that of untreated cells. **D-E**. Collateral

sensitivity of caspofungin-evolved strains with FK20 RPM **(D.)**, and FK20-evolved strains to caspofungin. Each data point represents the mean ± S.E calculated from three lineages in three independent experiments performed in triplicates.

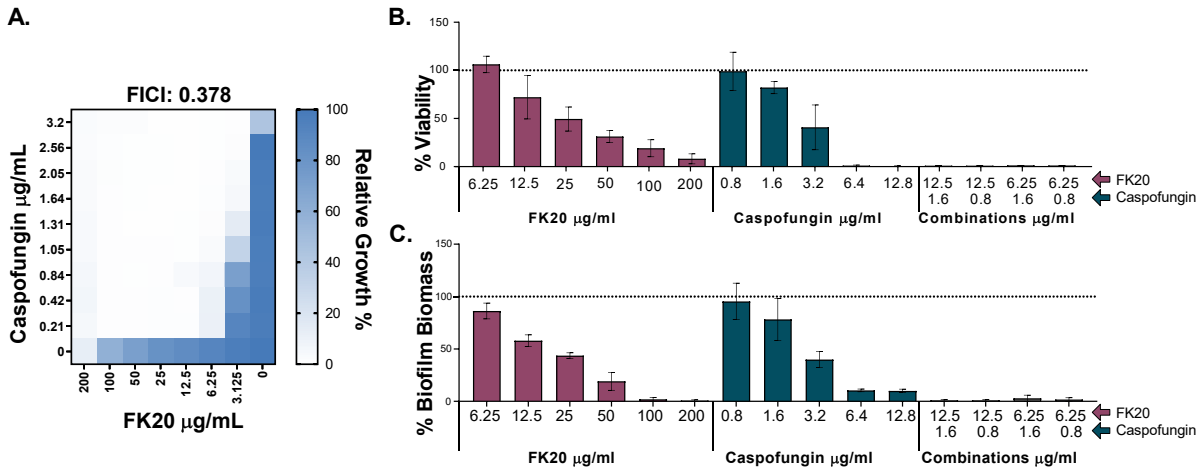

Figure 7: Synergistic effect of FK20 and caspofungin on *C. auris* biofilm formation. A. Combined effects of FK20 and caspofungin on *C. auris* cells. The Fractional Inhibitory Concentration (FICI) Index was determined using a checkerboard assay. The heat map illustrates the percentage growth of *C. auris* under various combinations of caspofungin and FK20 concentrations. B-C. Inhibition of *C. auris* biofilm formation by FK20, caspofungin, and their combination, quantified via MTT (B) and crystal violet (C) after 24 hours. FK20 and caspofungin were included in the growth medium from the beginning of the experiment. The data are derived from three biologically independent experiments conducted in six replicates. Error bars represent SEM.

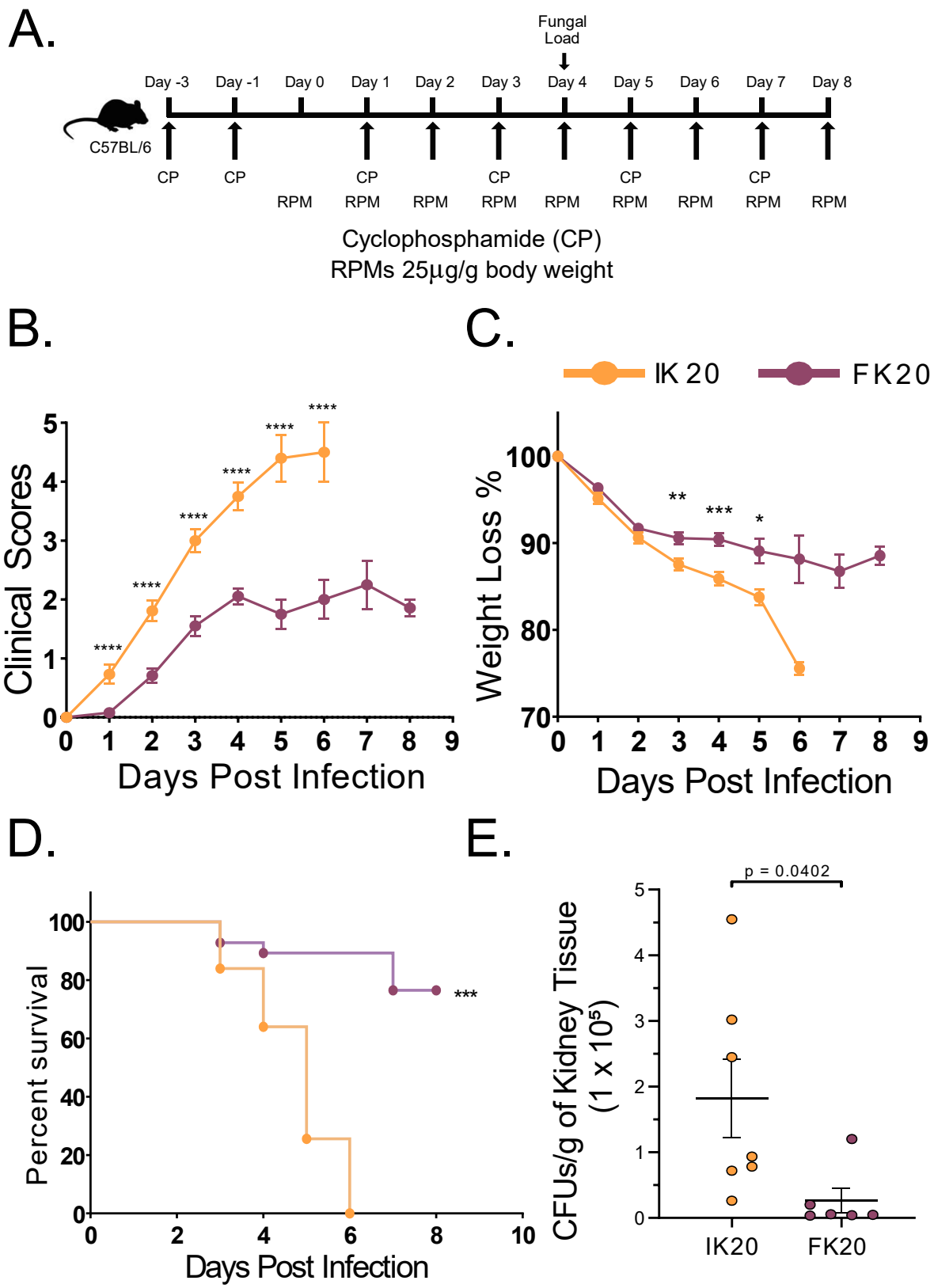

Figure 8: FK20 is fungicidal in a murine model of systemic candidiasis. A. An illustration of the timeline of infection in a murine model of systemic candidiasis. Groups of C57Bl/6 Mice were immunosuppressed using cyclophosphamide, then infected intravenously with 1 x 10^6 CFUs of *C. auris.* Throughout the experiment, they were treated with daily intramuscular injections of either 25 µg/gr

FK20 or IK20 RPMs. **B-C.** Clinical scores **(B)** & Percentage weight loss **(C)** reflecting disease severity were determined from observations of physical activity and weight changes respectively of mice infected with *C. auris* then treated with FK20 or IK20. **D**. Percentage of mice survival. **E.** Fungal burden in kidneys of infected and treated mice. Error bars represent SEM for n = 7 (IK 20) and n = 6 (FK20). Significance was determined with t test; $p < 0.05$.

Supplementary Data

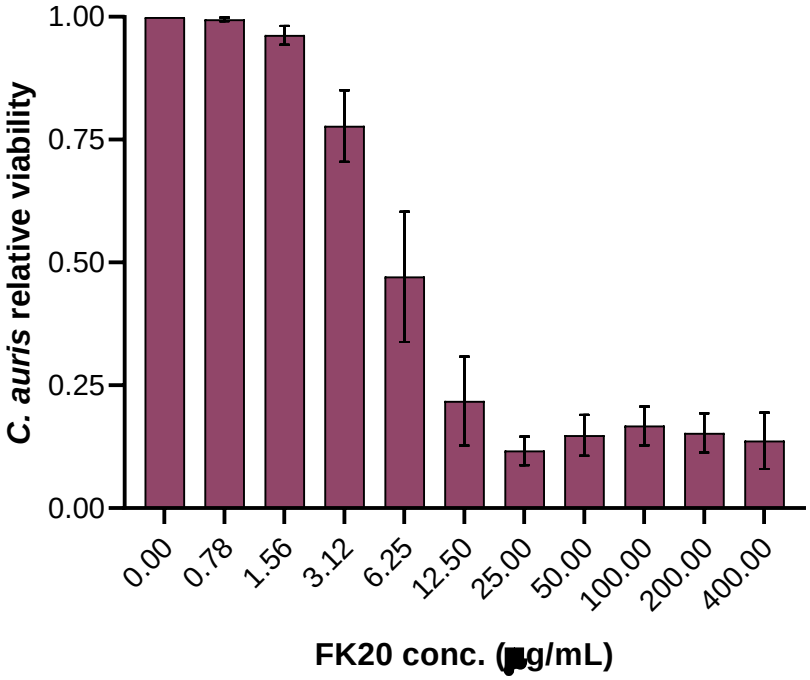

Figure S1: Membrane damage quantification by ghost dye staining. *C. auris* cells were incubated with FK20 RPM at concentration ranging from 0 – 400 µg/mL for 45 minutes at 37°C with continuous shaking. Membrane damage was evaluated by staining *C. auris* cells with Ghost dye for 20 minutes. Cell viability was determined by measuring Ghost dye fluorescence using a flow cytometer. The viability of *C. auris* was calculated as the percentage of cells that remained unstained by Ghost dye relative to the untreated control. The data are derived from three biologically independent experiments conducted in triplicates.

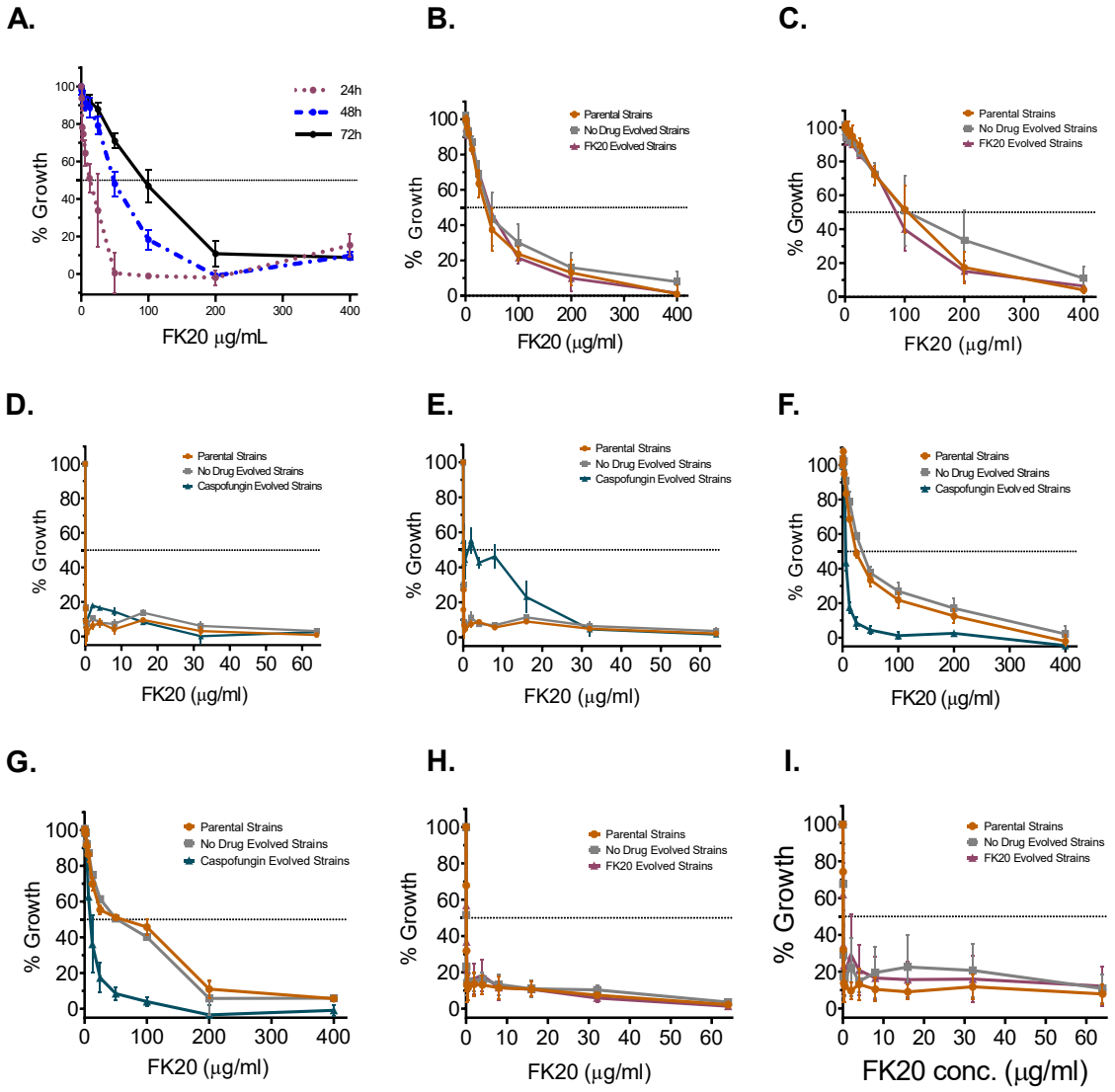

Figure S2: In vitro-experimental evolution. A. Initial MIC-50 of FK20 determined on a growth curve of *C.auris* treated with a range of concentrations from 0-400µg/ml FK20. **B-I**. Growth curves of different strains under drug treatment are shown. Panels B and C display the growth of parental, ND-evol, and FK20-evolved strains treated with FK20 at 24 and 48 hours, respectively. Panels D and E depict the growth of parental, ND-evol, and caspofungin-evolved strains treated with caspofungin at 24 and 48 hours. Additionally, panels F and G show the response of parental, ND-evol, and FK20-evolved strains to caspofungin at 24 and 48 hours, while panels H and I illustrate the growth of parental, ND-evol, and caspofungin-evolved strains in response to FK20 at 24 and 48 hours.

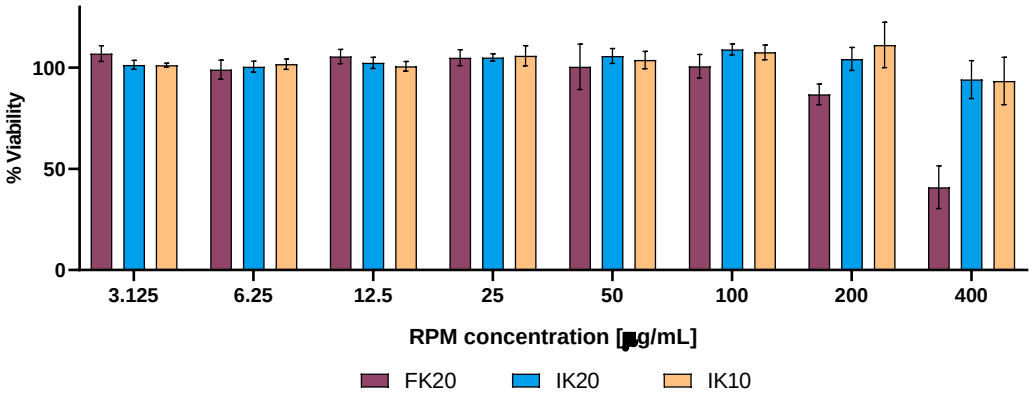

Figure S3: RPMs exhibit no cytotoxicity in cultured cells. RAW 264.7 murine macrophage cells were incubated with FK20, IK20, or IK10 for 24 hours at 37°C in a 5% CO_2 environment. Cell viability was assessed using the MTT assay, with macrophage viability expressed relative to a control group with no treatment. The data represents the mean of three biologically independent experiments, each performed in triplicate.

Test	UPW	IK10	FK20	Reference values
AST (IU/L)	246.5 ± 341.5	81 ± 187	90 ± 275	57-329
ALT (IU/L)	20 ± 38	3 ± 28	6 ± 32	22-133
ALP (IU/L)	13.5 ± 141.5	12.5 ± 110.5	12 ± 94	16-200
GGT (IU/L)	3 >	3 >	3 >	3 >

Table S1: Hematology Profiles and Blood Chemistry. A control group of Mice were administered ultra-pure water, FK20 or IK10 RPMs intramuscularly daily for four days (25 µg/gr body weight). Hematology and blood chemistry was analyzed on day four. n=5 per group.

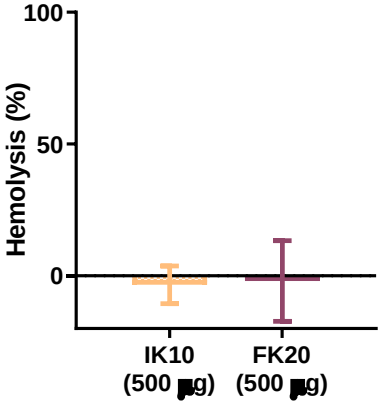

Figure S4: RPMs are not hemolytic. A control group of Mice were administered ultra-pure water, FK20 or IK10 RPMs intramuscularly daily for four days (25 µg/gr body weight). Hemolysis was analyzed on day four by direct spectrophotometric measurement at 540 nm. n=5 per groups.